2013

THz photomixer with a 40-nm-wide nanoelectrode gap on low-temperature grown GaAs

G Seniutinas
Swinburne University of Technology

G Gervinskas
Swinburne University of Technology

E Constable
University of Wollongong, evanc@uow.edu.au

A Krotkus
Center for Physical Sciences and Technology

G Molis
Teravil Ltd

See next page for additional authors

Publication Details

Seniutinas, G., Gervinskas, G., Constable, E., Krotkus, A., Molis, G., Valusis, G., Lewis, R. A. & Juodkazis, S. (2013). THz photomixer with a 40-nm-wide nanoelectrode gap on low-temperature grown GaAs. In J. Friend & H. Hoe. Tan (Eds.), Proceedings of SPIE (pp. 892322-1-892322-9). United States: SPIE.

THz photomixer with a 40-nm-wide nanoelectrode gap on low-temperature grown GaAs

Abstract
A terahertz (THz or T-rays) photomixer consisting of a meander type antenna with integrated nanoelectrodes on a low temperature grown GaAs (LT-GaAs) is demonstrated. The antenna was designed for molecular fingerprinting and sensing applications within a spectral range of 0.3-0.4 THz. A combination of electron beam lithography (EBL) and focused ion beam (FIB) milling was used to fabricate the T-ray emitter. Antenna and nanoelectrodes were fabricated by standard EBL and lift-off steps. Then a 40-nm-wide gap in an active photomixer area separating the nanoelectrodes was milled by a FIB. The integrated nano-contacts with nano-gaps enhance the illuminated light and THz electric fields as well as contribute to a better collection of photo-generated electrons. T-ray emission power from the fabricated photomixer chips were few hundreds of nanowatts at around 0.15 THz and tens of nanowatts in the 0.3-0.4 THz range.

Keywords
40, nm, thz, temperature, low, gaas, gap, nanoelectrode, wide, grown, photomixer

Disciplines
Engineering | Physical Sciences and Mathematics

Publication Details
Seniutinas, G., Gervinskas, G., Constable, E., Krotkus, A., Molis, G., Valusis, G., Lewis, R. A. & Juodkazis, S. (2013). THz photomixer with a 40-nm-wide nanoelectrode gap on low-temperature grown GaAs. In J. Friend & H. Hoe. Tan (Eds.), Proceedings of SPIE (pp. 892322-1-892322-9). United States: SPIE.

Authors
G Seniutinas, G Gervinskas, E Constable, A Krotkus, G Molis, G Valusis, Roger A. Lewis, and S Juodkazis

THz photomixer with a 40-nm-wide nanoelectrode gap on a low-temperature grown GaAs

G. Seniutinas[a,b], G. Gervinskas[a,b], E. Constable[c], A. Krotkus[d], G. Molis[e], G. Valušis[d], R. A. Lewis[c], and S. Juodkazis[a,b]

[a]Centre for Micro-Photonics, Faculty of Engineering and Industrial Sciences, Swinburne University of Technology, Hawthorn, VIC 3122, Australia
[b] Melbourne Centre for Nanofabrication, Australian National Fabrication Facility, Clayton, VIC 3168, Australia
[c]Institute for Superconducting and Electronic Materials, University of Wollongong, Wollongong, NSW 2522, Australia;
[d]Center for Physical Sciences and Technology, Vilnius, LT 01108, Lithuania;
[e]Teravil Ltd, Vilnius, LT 01108, Lithuania

ABSTRACT

A terahertz (THz or T-rays) photomixer consisting of a meander type antenna with integrated nanoelectrodes on a low temperature grown GaAs (LT-GaAs) is demonstrated. The antenna was designed for molecular fingerprinting and sensing applications within a spectral range of 0.3-0.4 THz. A combination of electron beam lithography (EBL) and focused ion beam (FIB) milling was used to fabricate the T-ray emitter. Antenna and nanoelectrodes were fabricated by standard EBL and lift-off steps. Then a 40-nm-wide gap in an active photomixer area separating the nanoelectrodes was milled by a FIB. The integrated nano-contacts with nano-gaps enhance the illuminated light and THz electric fields as well as contribute to a better collection of photo-generated electrons. T-ray emission power from the fabricated photomixer chips were few hundreds of nanowatts at around 0.15 THz and tens of nanowatts in the 0.3-0.4 THz range.

Keywords: Terahertz, photomixer, nanoelectrodes, low temperature GaAs

1. INTRODUCTION

Terahertz technology shows considerable potential in many applications, including medical imaging, security screening, real time production testing, wireless communications, and many others.[1–7] However, a lack of compact and powerful emitters of T-rays has limited widespread utilization of this technology. A lot of effort to create compact and efficient THz sources have been expended during the last decades and different generation techniques based on free electron acceleration,[8] laser effects (quantum cascade lasers (QCL's),[9] germanium lasers[10]), optical rectification,[11] and photoconductive effects (photoconductive switch,[12] photomixers[13]) have been proposed. Each approach has its own advantages and drawbacks. For example, free electron lasers offer high power emission but they need a high vacuum for operation and the whole system is very bulky. QCL's are very compact in their dimensions and produce THz radiation in the mW range[14] but they need cryogenic cooling for operation.

Photomixing devices can operate at room temperature, are easily tunable and compact, all this is of benefit to most practical applications. Theoretically, extremely high optical-to-THz conversion efficiencies may be obtained in photoconductive mixers, as the emitted energy comes from the accelerating bias electric field; thus one electron-hole pair created by pump laser can generate many T-ray photons.[15] However, the achievable conversion efficiency is still well below theoretical values due to antenna impedance mismatch and poor photogenerated carrier collection. Despite of a lower power, photoconductive antenna emitters are common sources of pulsed and continuous wave THz radiation.

Send correspondence to G. S.: GSeniutinas@swin.edu.au
Further author information: Valusis@pfi.lt (GV), Roger@uow.edu.au (RAL), SJuodkazis@swin.edu.au (SJ).

Micro/Nano Materials, Devices, and Systems, edited by James Friend, H. Hoe Tan, Proc. of SPIE
Vol. 8923, 892322 · © 2013 SPIE · CCC code: 0277-786X/13/$18 · doi: 10.1117/12.2033746

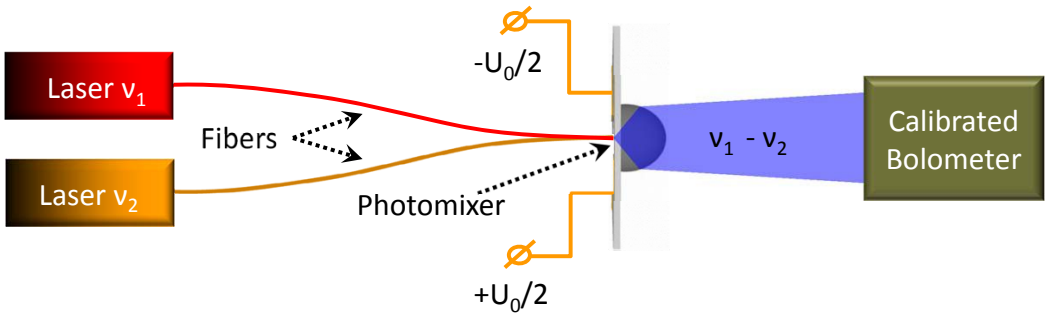

Figure 1. (color online) Schematics of the used characterization scheme: lasers were operating at around $\lambda \approx 850$ nm wavelengths (frequencies $\nu_{1,2} = c/\lambda_{1,2}$).

To improve the conversion efficiency and boost the photomixer emitted T-ray power, different nanostructures such as nanoelectrodes[16] and nanogratings,[16–19] as well as new antenna designs,[20] have been introduced. Integrated nanostructures employ plasmonic effects to increase pump laser intensity near nanostructures, generating more carriers in these regions and, also, enhancing the electric field of the generated THz wave. Moreover, nanostructures cover most of the active area providing a better collection of photo-generated carriers and feeding of antenna current.

Here, we demonstrate fabrication of photomixers with integrated nanoelectrodes operating at the mixing wavelengths longer than 800 nm using combined nano-lithographical approaches on LT-GaAs substrates. Meander THz antennas, designed for emission in a 0.3-0.4 THz range, and sub-100 nm gold nanoelectrodes were patterned using electron beam lithography (EBL) and standard lift-off procedures. Then, a 40-nm-wide plasmonic gap was opened by direct focused ion beam (FIB) milling of the fabricated contacts. We show the current fabrication limits of the nanoelectrodes. THz emission of the fabricated photomixers is demonstrated.

2. EXPERIMENTAL: FABRICATION AND CHARACTERIZATION

2.1 Photo-mixer fabrication

Molecular beam epitaxially grown LT-GaAs was chosen as the photoconductive substrate. It is a common material for THz emitters due to its high dark resistivity, sub-picosecond carrier lifetime and high carrier mobility. Photomixer structures with 100 nm wide nanoelectrodes were fabricated using EBL (Raith 150^{TWO}) and nanogroove was milled by applying FIB lithography system (Raith, IonLiNE). Scanning electron microscopy (SEM) and FIB sectioning (FEI Helios dual beam) of the nano-contact areas were utilised for morphology inspection.

2.2 Characterization of THz emission

A simplified THz emission characterization scheme is shown in Fig. 1. Two continuous-wave tunable DFB (Toptica) semiconductor lasers operating at central wavelengths of around 850 nm served as sources for mixing wavelengths. The mixing beams were combined in a fiber and fed into a semiconductor amplifier (Toptica BoosTA). The amplified beam was directed onto the active photomixer area via a fiber coupled to a collimating lens. The position of the beam was optimized using a 3-axis stage and maximizing the output signal. An oscilating bias voltage of 183 Hz with amplitude changing from 0 V to U_0 was applied to the photomixer. A calibrated liquid He-cooled bolometer was used as a detector of the emitted T-rays. The bolometer signal was detected using a lock-in amplifier synchronised for for the same frequency as oscilating voltage (183 Hz). The THz emission spectra was recorded by changing the beat frequency between mixing wavelengths. The emission frequency of one laser was fixed at 852 nm while the frequency of the second laser was tuned by precisely changing its operating temperature. The power was estimated by using a bolometer responsivity of 10^5 V/W and should only be regarded as approximate.

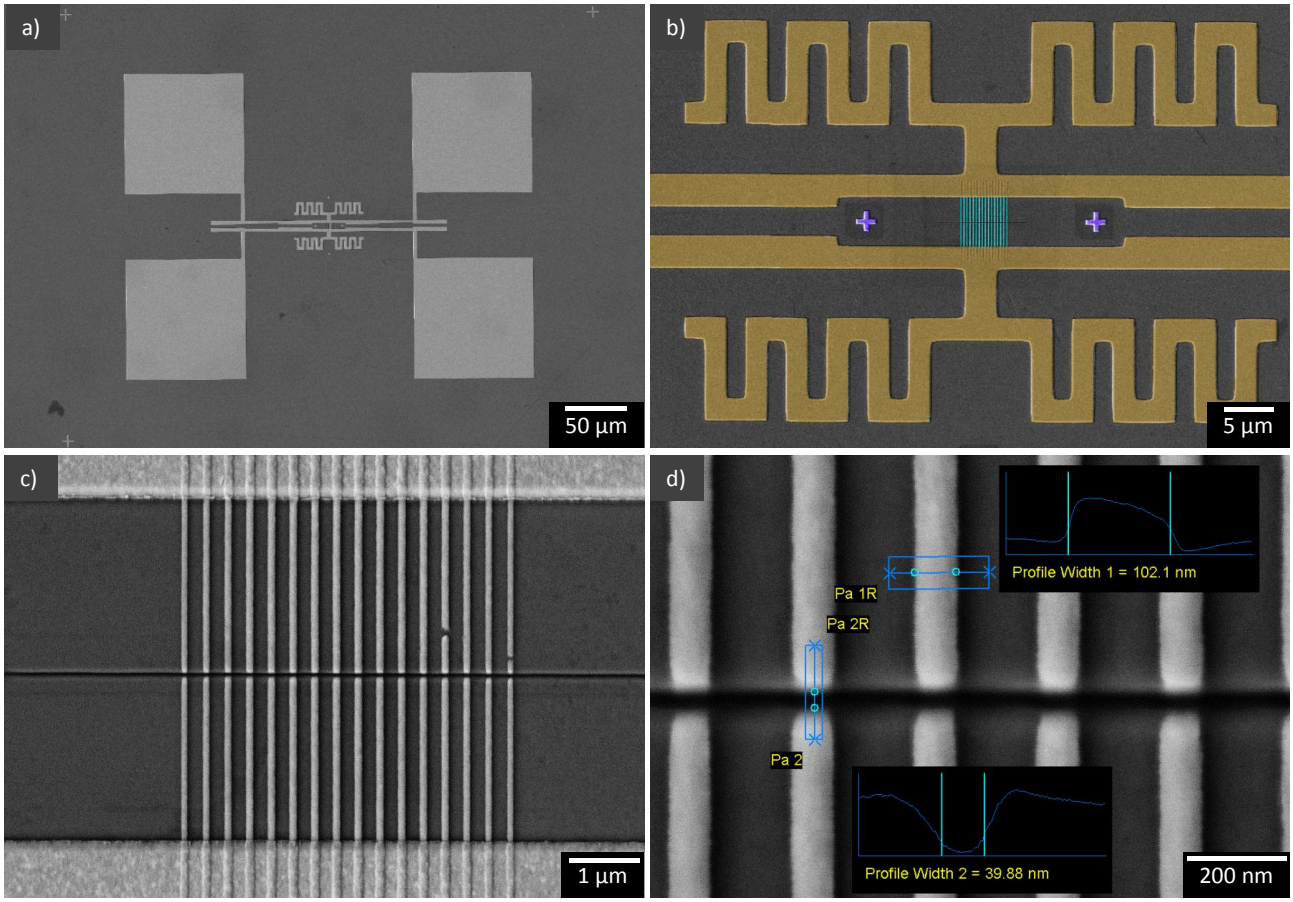

Figure 2. (color online)SEM images of the THz photomixer on LT-GaAs chip: a) antenna with contact pads for bias voltage; b) zoomed in meander antenna with nanoelectrodes, crosses are the alignment marks for ion beam milling step; c) nanoelectrodes for electric field enhancement and better carrier collection; d) 40-nm-wide gap between electrodes was milled with FIB.

3. RESULTS

First, the fabrication of the photomixers with nano-gap electrodes and its structural composition are described and, then, their performance as THz emitters as well as current-voltage characteristics are discussed.

3.1 Photo-mixers with nano-gaps

The fabricated structure composed of the bias voltage contact pads and antenna with nanoelectrodes is shown in Fig. 2(a). Two fabrication approaches were tested to define the emitter regions of the structures.

The first one was to use a two-step method for fabrication of nanostructures and antenna (Fig. 2(b)). This approach employs two steps of the EBL fabrication procedures. First, nanoelectrodes were patterned in a positive polymethyl methacrylate (PMMA) resist and the created openings in the PMMA mask then was sputtered with 5 nm Ti adhesion layer and 25 nm Au for nanoelectrodes. The standard lift-off procedure in acetone was used to remove the PMMA mask. The following step was to coat PMMA resist again, precisely align antenna pattern on top of the nanostructures made earlier and to repeat the patterning by EBL and lift-off.

The second approach used a single EBL step. The nanoelectrodes and antenna masks were fabricated in one run on the same PMMA layer and then 10 nm Ti and 150 nm Au layers were deposited following the lift-off. Even though the patterned designs were the same for both methods, the actual structures varied. As shown in Fig. 3, the structure fabricated in two steps (marked as photomixer #1) had well-defined nanostructures (as designed), while nanoelectrodes made in one EBL step (marked as photomixer #2) had a strong tapering. This

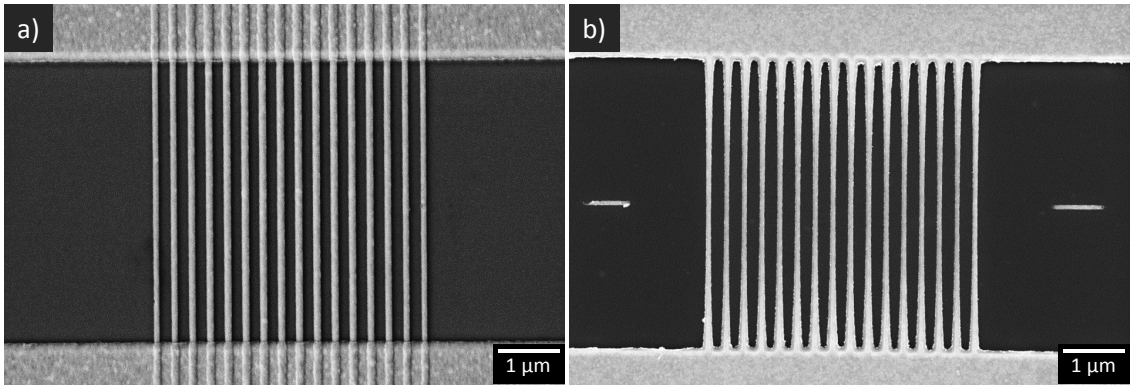

Figure 3. (color online) Photomixer nanoelectrodes prior ion beam milling: a) two-step EBL process (device #1); b) one-step EBL process (device #2).

is a known proximity effect in EBL patterning and can be corrected using process simulation software. Since proximity correction requires a sophisticated exposure control we were not using it in our fabrication routine.

The bias voltage is required for acceleration of the photo-generated carriers and to drive them to the antenna. To have an electric field in the active region there is a need to isolate the two antenna sides from each other. For this reason focused Ga-ion beam milling was used. It allows the cutting of a nanometer sized gap in the nanoelectrodes and to electrically isolate the two antenna sides. The gap can be also formed during the EBL process but it is more difficult to reach separation widths of several nanometers between wider electrodes and, at the same time, to have a good edge quality for the plasmonic enhancement. The milled 40 nm wide groove is shown in Fig. 2(c,d). Ion beam milling is a separate additional step in photomixer fabrication, and the cut should be aligned exactly at the middle of nanoelectrodes. For this reason, additional alignment marks (crosses in Fig.2(b)) were fabricated during the EBL process. These crosses serve as reference points for precise cutting with a FIB. Since the FIB is a direct write method, it is a simplified fabrication step as compared with an EBL definition of nano-gaps.

LT-GaAs chips with the fabricated photomixers were mounted on printed circuit boards (PCB, Fig. 4) for the characterization of THz emission. A hyper-hemispherical high resistance Si lens (Tydex) was aligned, centered and glued on the backside of the chip for collimation of the emitted T-rays. Electrical contacts connecting the PCB board and the photomixer were made by application of conductive silver paint.

Cross sectioning of the fabricated photomixer was used to inspect the structural composition of photo-mixer (Fig. 5). According to the standard procedure, a protective Pt layer was deposited on a cross section region

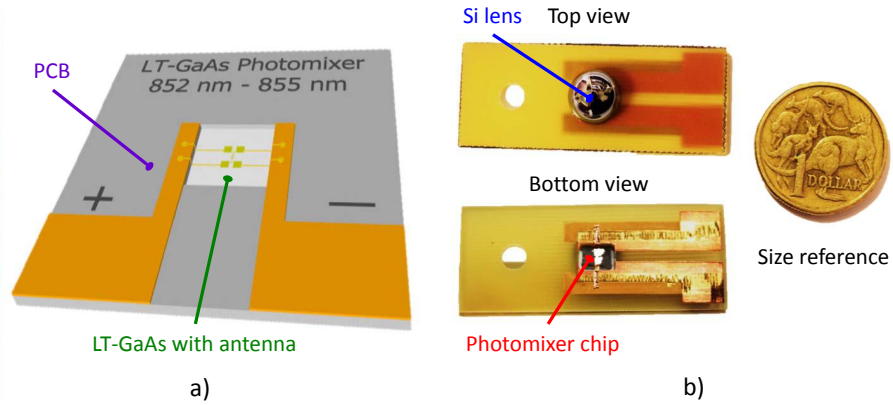

Figure 4. (color online) a) Designed photomixer chip mounting on PCB board; b) photomixer chip mounted on PCB board. Hyper-hemispherical Si lens was used for T-ray collimation.

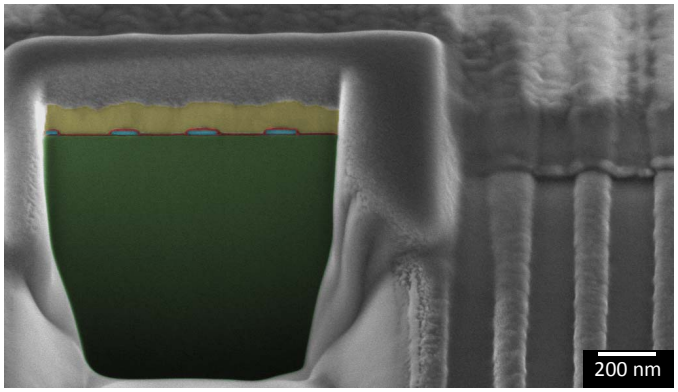

Figure 5. (color online) Cross-section of photomixer #1: 25 nm thick Au nanoelectrodes, followed by titanium adhesion layer, 150-nm-thick Au antenna layer, and a LT-GaAs substrate. The cross-section region was covered by Pt layer.

to maintain the boundaries of overlapped structures unaltered by milling. As shown in Fig. 5, 25 nm thick nanocontact tips fabricated during the first EBL step were buried under a 150 nm Au antenna layer forming an electrical contact for the photo-generated carriers.

3.2 T-ray emission from photo-mixers

First, current-voltage characteristics of the active photomixer area were measured (Fig. 6). As dark resistivity of the LT-GaAs substrate is high, the dark current (no photo-excitation) in the active region is by a few orders of magnitude lower than the photo-current. The gap between nanoelectrodes is tens-of-nanometers and this facilitates to reach high electric field values in the gap even at low bias voltages ($\sim$ 250 kV/cm at 1 V bias). A super-linear dependance of the current-voltage (I-V) curves was obtained (Fig. 6). It can be explained by an increase of the carrier lifetime and Coulomb-barrier reduction at high electric fields near the collection electrodes.[21] Also, a recombination-limited transport of photo-excited carriers is another possibility.[22] Further studies are required for a distinct clarification of the mechanism and its current dependence.

Next, T-ray emission spectra and power dependences on the laser excitation power was measured (Fig. 7(a)). In ideal case, the antenna emitted power can be found using Ohm's law. From Ohm's law for time-varying currents, the average power is:

$$P_{THz} = R_A {I_{avg}}^2, \tag{1}$$

here, R_A is the antenna resistance and I_{avg} is current flowing in antenna average. The beat frequency modulated current can be written as periodic function of transient current (I_{THz}) due to photo-generated carriers:

$$I = I_{THz} \cos(\omega_{THz} t). \tag{2}$$

I_{THz} depends on pump laser power as:

$$I_{THz} = \frac{eP_p}{h\nu}, \tag{3}$$

where $h\nu$ is the bandgap energy of photo-conductor (LT-GaAs in this case), P_p is the cumulative pump power of the mixing beams, and e is the electron charge. The antenna emitted terahertz power dependance on laser pump power is obtained by taking temporal average of Eq.2 and inserting it in Eq.1:

$$P_{THz} = \frac{1}{2} R_A {I_{THz}}^2 = \frac{1}{2} R_A \left(\frac{eP_p}{h\nu}\right)^2. \tag{4}$$

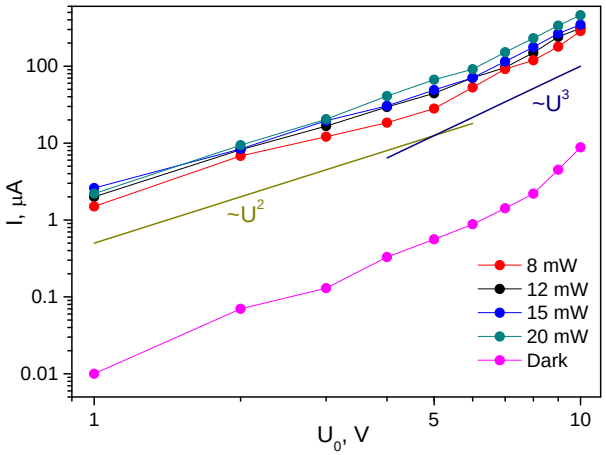

Figure 6. Photo-current vs bias voltage (I-V) from the LT-GaAs chip at different power of the laser illumination; note, lg – lg presentation. Scalling $I \propto U^2$, U^3 are shown.

This quadratic scaling of the emitted power on the power of the pump laser $P_{THz} \sim P_p^2$ is plotted as an eye guide in Fig. 7(b). As expected, the radiated T-ray power increases quadratically with respect to the power of the mixing beams from 20 to 55 mW. The nanoelectrodes were damaged after the pump power was larger than 55 mW. The strongest THz emission of the photomixers was observed in the spectral range of 0.1 - 0.2 THz. The emission spectra for photomixers #1 and #2 are slightly different as shown in Fig. 8(a). Even though they both show emission peaks at around 0.1 and 0.15 THz, the first chip also showed emission in the 0.3 - 0.4 THz range (Fig.8b inset), the range this photomixer was designed for. The second device did not have a detectable signal in that range. This could be due to a better impedance matching and antenna quality of the first photomixer, as it was fabricated in two EBL steps and the electrodes had no tapering.

4. DISCUSSION

The Terahertz field is under active development and attracts a lot of research efforts due to its unique applications in sensing. The bottle neck of T-ray technology is in emitters where better materials have to be developed together with improved antenna designs and fabrication methods. The photomixers reported here require further

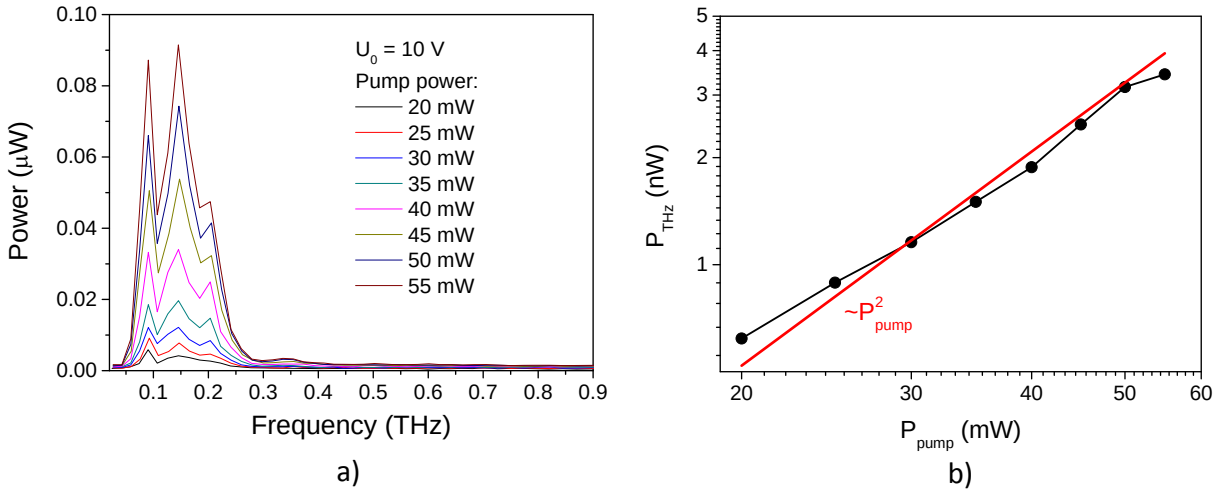

Figure 7. a)Photomixer #1 emission spectra dependence on laser pump power at 10 V bias voltage; b) quadratic power dependence.

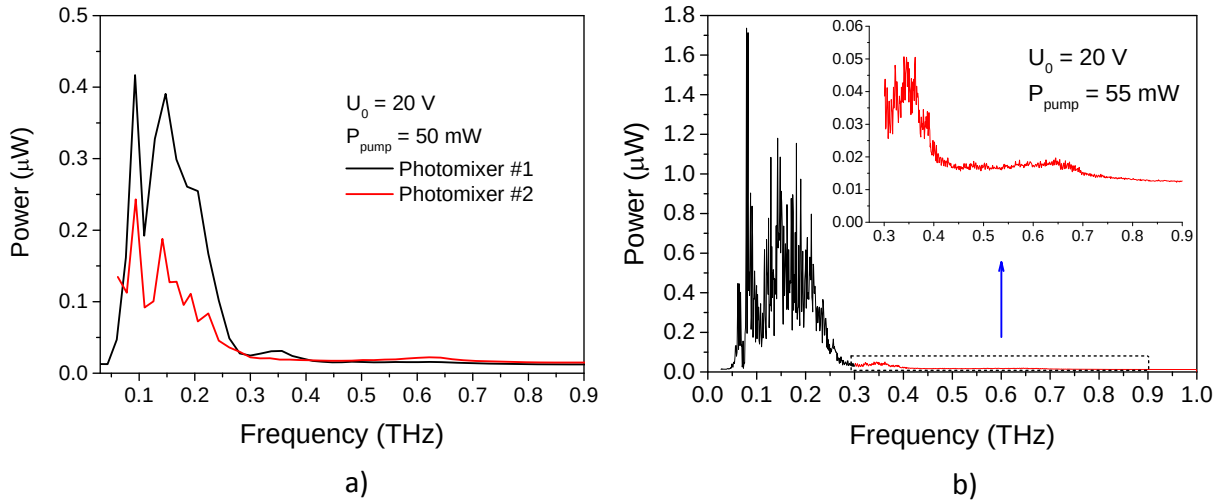

Figure 8. a) Comparison of spectra emitted by #1 and #2 photomixer chips. b) A higher resolution spectrum from the photomixer #1 at a 20 V bias and under a 55 mW illumination laser power.

improvements in the power output and repeatability of fabrication. Impedance matching is one of the major challenges to overcome for enhancing the T-ray emission.

The use of nanoelectrodes and nanogratings in antenna designs assist in exploiting the plasmonic effect of light field enhancement of the mixed wavelength illumination in the subsurface and near-electrode regions as well as an enhancement of the generated terahertz electric fields. Nanostructures trenched into the substrate could be a further step in fabrication improvement of a next generation of photomixers. The nano-gaps and light field enhancing nano-features (creation of nano-sharp corners between nanoparticles) can be made by EBL and lift-off[23–33] procedures. However, FIB milling of arbitrary shaped electrodes and substrate modifications at the closest proximity of the electrodes using a FIB is very appealing for future antenna designs.[26,34–36] Recently, we have demonstrated that charging effects during FIB can be compensated using UV exposure of the fabrication region during groove formation.[37] This further improves nano-structuring down to a 15-20 nm resolution which is expected to contribute to stronger light field enhancement especially at the wavelengths used for photo-mixing.

5. CONCLUSIONS

Fabrication of T-ray photomixer chips by combining EBL and FIB is demonstrated. Sub-50 nm nanoelectrode gaps were reliably fabricated on the nano-electrode arrays for the first time. The mixer was operational at the mixing wavelengths around 850 nm which were exciting photo-carriers and emitted power was estimated to be in order of hundreds of nanowatts at 0.15 THz and around one order lower in the 0.3-0.4 THz range.

Direct FIB writing of electrodes with nano-gaps, inscribing of fractal patterns for the enhancement of illuminating light beams at near-IR and IR wavelengths as well as the THz emitted fields can provide further optimization and enhancement of photomixers. Miniaturization of photomixers at a 0.3-0.7 THz wavelengths is promising in security,[38] forensic, and medical[39,40] applications.

ACKNOWLEDGEMENTS

We are grateful for support via Australian Research Council Discovery DP130101205 and DP120102980 grants. The PhD scholarship of GS is funded via the ARC Linkage grant LP120100161 with Raith-Asia. The THz experimental setup was supported by the Australian Research Council and the University of Wollongong.

REFERENCES

1. N. Katzenellenbogen and D. Grischkowsky, "Electrical characterization to 4 THz of N-and P-type GaAs using THz time-domain spectroscopy," *Appl. Phys. Lett.* **61**(7), pp. 840–842, 1992.

2. J. Bjarnason, T. Chan, A. Lee, M. Celis, and E. Brown, "Millimeter-wave, terahertz, and mid-infrared transmission through common clothing," *Appl. Phys. Lett.* **85**(4), pp. 519–521, 2004.
3. A. Lee and Q. Hu, "Real-time, continuous-wave terahertz imaging by use of a microbolometer focal-plane array," *Opt. Lett.* **30**(19), pp. 2563–2565, 2005.
4. Y. Jin, G. Kim, and S. Jeon, "Terahertz dielectric properties of polymers," *J. Korean Phys. Soc.* **49**(2), pp. 513–517, 2006.
5. B. Fischer, H. Helm, and P. Jepsen, "Chemical recognition with broadband THz spectroscopy," *Proc. IEEE* **95**(8), pp. 1592–1604, 2007.
6. W. Stillman, D. Veksler, T. Elkhatib, K. Salama, F. Guarin, and M. Shur, "Sub-terahertz testing of silicon MOSFET," *Electronics Lett.* **44**(22), pp. 1325–1326, 2008.
7. B. St.Peter, S. Yngvesson, P. Siqueira, P. Kelly, A. Khan, S. Glick, and A. Karellas, "Development and testing of a single frequency terahertz imaging system for breast cancer detection," *Terahertz Sci. Techn., IEEE Trans.* **3**(4), pp. 374–386, 2013.
8. G. L. Carr, M. C. Martin, W. R. McKinney, K. Jordan, G. R. Neil, and G. P. Williams, "High-power terahertz radiation from relativistic electrons," *Nature* **420**(6912), pp. 153–156, 2002.
9. J. Faist, F. Capasso, D. L. Sivco, C. Sirtori, A. L. Hutchinson, and A. Y. Cho, "Quantum cascade laser," *Science* **264**(5158), pp. 553–556, 1994.
10. H. Hübers, S. Pavlov, and V. Shastin, "Terahertz lasers based on germanium and silicon," *Semiconductor Sci. Tech.* **20**(7), p. S211, 2005.
11. K.-L. Yeh, M. Hoffmann, J. Hebling, and K. A. Nelson, "Generation of 10 μj ultrashort terahertz pulses by optical rectification," *Appl. Phys. Lett.* **90**, p. 171121, 2007.
12. D. Auston, K. Cheung, and P. Smith, "Picosecond photoconducting Hertzian dipoles," *Appl. Phys. Lett.* **45**(3), pp. 284–286, 1984.
13. E. Brown, K. McIntosh, K. Nichols, and C. Dennis, "Photomixing up to 3.8 THz in low-temperature-grown GaAs," *Appl. Phys. Lett.* **66**(3), pp. 285–287, 1995.
14. C. Sirtori, S. Barbieri, and R. Colombelli, "Wave engineering with THz quantum cascade lasers," *Nature Phot.* **7**(9), pp. 691–701, 2013.
15. S. Preu, G. Döhler, S. Malzer, L. Wang, and A. Gossard, "Tunable, continuous-wave Terahertz photomixer sources and applications," *J. Appl. Phys.* **109**, p. 061301, 2011.
16. H. Tanoto, J. Teng, Q. Wu, M. Sun, Z. Chen, S. Maier, B. Wang, C. Chum, G. Si, A. Danner, *et al.*, "Nano-antenna in a photoconductive photomixer for highly efficient continuous wave Terahertz emission," *Sci. Rep.* **3**, 2013.
17. C. Berry, M. Unlu, M. Hashemi, and M. Jarrahi, "Use of plasmonic gratings for enhancing the quantum efficiency of photoconductive Terahertz sources," in *Infrared, Millimeter, and Terahertz Waves (IRMMW-THz), 2012 37th Int. Conf.*, pp. 1–2, IEEE, 2012.
18. C. Berry and M. Jarrahi, "Terahertz generation using plasmonic photoconductive gratings," *New J. Phys.* **14**(10), p. 105029, 2012.
19. C. Berry, N. Wang, M. Hashemi, M. Unlu, and M. Jarrahi, "Significant performance enhancement in photoconductive terahertz optoelectronics by incorporating plasmonic contact electrodes," *Nature Comm.* **4**, p. 1622, 2013.
20. K. Pitra, Z. Raida, and H. Hartnagel, "Design of circularly polarized Terahertz antenna with interdigital electrode photomixer," in *Antennas and Propagation (EuCAP), 2013 7th European Conf.*, pp. 2431–2434, 2013.
21. N. Zamdmer, Q. Hu, K. McIntosh, and S. Verghese, "Increase in response time of low-temperature-grown GaAs photoconductive switches at high voltage bias," *Appl. Phys. Lett.* **75**(15), pp. 2313–2315, 1999.
22. E. Brown, K. McIntosh, F. Smith, K. Nichols, M. Manfra, C. Dennis, and J. Mattia, "Milliwatt output levels and superquadratic bias dependence in a low-temperature-grown GaAs photomixer," *Appl. Phys. Lett.* **64**(24), pp. 3311–3313, 1994.
23. S. Juodkazis and L. Rosa, "Surface defect mediated electron hopping between nanoparticles separated by a nano-gap," *Phys. Stat. Sol. - rapid research letters* **4**(10), pp. 244–246, 2010.

24. L. Rosa, K. Sun, J. Szymanska, F. E. Hudson, A. Dzurak, A. Linden, S. Bauerdick, L. Peto, and S. Juodkazis, "Tailoring spectral position and width of field enhancement by ion-beam trimming of plasmonic nanoparticles," *Phys. Stat. Sol. - rapid research letters* **4**(10), pp. 262 – 264, 2010.
25. C.-H. Poh, L. Rosa, S. Juodkazis, and P. Dastoor, "FDTD modeling to enhance the performance of an organic solar cell embedded with gold nanoparticles," *Opt. Mater. Express* **1**, pp. 1326–1331, 2011.
26. L. Rosa, K. Sun, and S. Juodkazis, "Serpinski fractal plasmonic nanoantennas," *Phys. Stat. Sol. - rapid research letters* **5**(5-6), pp. 175–177, 2011.
27. Y. Nishijima, L. Rosa, and S. Juodkazis, "Surface plasmon resonances in periodic and random patterns of gold nano-disks for broadband light harvesting," *Opt. Express* **20**(10), pp. 11466–11477, 2012.
28. Y. Nishijima, H. Nigorinuma, L. Rosa, and S. Juodkazis, "Selective enhancement of infrared absorption with metal hole arrays," *Opt. Mat. Express* **2**(10), pp. 1367–1377, 2012.
29. G. Seniutinas, L. Rosa, G. Gervinskas, E. Brasselet, and S. Juodkazis, "3D nano-structures for laser nano-manipulation," *Beilstein J. Nanotechn.* , 2013 (in press).
30. Y. Nishijima, J. B. Khurgin, L. Rosa, H. Fujiwara, and S. Juodkazis, "Randomization of gold nano-brick arrays: a tool for SERS enhancement," *Opt. Express* **21**(11), pp. 13502–13514, 2013.
31. S. Jayawardhana, L. Rosa, S. Juodkazis, and P. R. Stoddart, "Additional enhancement of electric field in surface-enhanced Raman scattering due to Fresnel mechanism," *Sci. Rep.* **3**, p. 2335, 2013.
32. M. M. Islam, K. Ueno, S. Juodkazis, Y. Yokota, and H. Misawa, "Development of interdigitated array electrodes with SERS functionality," *Anal. Sci.* **26**, pp. 13–18, 2010.
33. K. Ueno, S. Juodkazis, T. Shibuya, V. Mizeikis, Y. Yokota, and H. Misawa, "Nano-particle-enhanced photo-polymerization," *J. Phys. Chem. C* **113**, pp. 11720–11724, 2009.
34. S. Juodkazis, L. Rosa, S. Bauerdick, L. Peto, R. El-Ganainy, and S. John, "Sculpturing of photonic crystals by ion beam lithography: towards complete photonic bandgap at visible wavelength," *Opt. Express* **19**(7), pp. 5802–5810, 2011.
35. L. Rosa, K. Sun, V. Mizeikis, S. Bauerdick, L. Peto, and S. Juodkazis, "3D-tailored gold nanoparticles for light field enhancement and harvesting over visible-IR spectral range," *J. Chem. Phys. C* **115**, pp. 5251–5256, 2011.
36. G. Gervinskas, G. Seniutinas, L. Rosa, and S. Juodkazis, "Arrays of arbitrarily shaped nanoparticles: Overlay-errorless direct ion write," *Adv. Opt. Mat.* **1**(6), pp. 456–459, 2013.
37. G. Gervinskas, G. Seniutinas, and S. Juodkazis, "Control of surface charge for high-fidelity nanostructuring of materials," *Laser Photonics Rev.* , pp. 1–5, 2013.
38. C. Zandonella, "Terahertz imaging: T-ray specs," *Nature* **424**(6950), pp. 721–722, 2003.
39. P. Knobloch, C. Schildknecht, T. Kleine-Ostmann, M. Koch, S. Hoffmann, M. Hofmann, E. Rehberg, M. Sperling, K. Donhuijsen, G. Hein, *et al.*, "Medical THz imaging: an investigation of histo-pathological samples," *Phys. Med. Biol.* **47**(21), p. 3875, 2002.
40. W. Baughman, H. Yokus, S. Balci, D. Wilbert, P. Kung, and S. Kim, "Observation of hydrofluoric acid burns on osseous tissues by means of Terahertz spectroscopic imaging," 2013.